Coincidence Imaging with a Dual-Head Scintillation Camera*

James A. Patton and Timothy G. Turkington

Department of Radiology and Radiological Sciences, Vanderbilt University Medical Center, Nashville, Tennessee; and the Department of Radiology, Duke University Medical Center, Durham, North Carolina

The feasibility of coincidence imaging of the annihilation radiation resulting from positron decay was demonstrated by Brownell and Sweet in 1953 (*1*), and the application of this technology using a dual-head scintillation camera was described as early as 1958 by Anger (*2,3*) and Anger and Rosenthal (*4*). Significant improvements in camera electronics led to the development of the Searle positron camera by Muehllehner in 1975 (*5*) and Muehllehner et al. (*6*). However, limitations in the counting rate capability of the scintillation camera and computer speed and algorithms for processing the resulting data initially prevented the development of systems with sufficient sensitivity to be clinically useful. Dedicated systems using coincidence detection in multiple small detectors arranged in hexagonal or circular arrays were developed to implement acceptable imaging capabilities, resulting in the modern day PET scanner (*7*). However, implementation of this technology has not been widespread because of the high cost of these systems, limited reimbursement, limited availability of positron-emitting tracers and the limitations of these dedicated systems to the imaging of positron emitters only.

Interest continued in the development of multipurpose systems that could be used for imaging positron emitters as well as routine single-photon emitters using large-field-of-view scintillation cameras commonly used in the nuclear medicine community. Parallel to the development of multicrystal systems, Muehllehner et al. (*6*) developed a PET system using large-area NaI(Tl) crystals. This system extended Anger camera principles to higher counting rates and improved efficiency (*8*). Similar but more compatible improvements to conventional scintillation camera technology during the past 4 y have now made it possible for manufacturers to implement coincidence detection techniques on a rotating dual-head scintillation camera (*9–11*). This dual-head coincidence (DHC) technology expands the potential for imaging positron tracers from the relatively small number of centers with dedicated PET scanners to the much larger number of centers that have chosen the coincidence imaging option on a recent gamma camera purchase.

Received Nov. 20, 1998; revision accepted Dec. 9, 1998.

For correspondence or reprints contact: James A. Patton, PhD, Department of Radiology and Radiological Sciences, Vanderbilt University Medical Center, 21st Ave. South and Garland, Nashville, TN 37232–2675.

*NOTE: FOR CE CREDIT, YOU CAN ACCESS THIS ARTICLE ON THE SNM WEB SITE (http://www.snm.org) UNTIL JUNE 1999.

CAMERA MODIFICATIONS

Manufacturers have devoted much effort in recent years to the optimization of the scintillation camera for low-energy imaging, because the vast majority of nuclear medicine procedures involve radionuclides with energies less than 200 keV. Because annihilation photons have an energy of 511 keV, the implementation of coincidence imaging with the scintillation camera has made it necessary to reverse some of these efforts and/or apply the technology that was developed for low-energy imaging to high-energy imaging applications.

The first step was to expand the pulse-height analyzer energy range. On some systems, the acquisition window is matched to the photopeak through high voltage adjustment. Systems such as this allow a wide range of acquisition energies. Other systems use a single high-voltage setting. For these systems, some manufacturers introduced a high-energy mode by simply reducing the high voltage and recalibrating the pulse height analyzer. This resulted in some difficulty in imaging at low energies (e.g., 70 keV for ^{201}Tl) when simultaneous imaging of low and high energies was desired. However, acceptable simultaneous collimated imaging at 140 and 511 keV has been successfully accomplished using this technique (*12,13*).

The energy dependence of flood field uniformity is well known, and manufacturers have typically used low- and medium-energy linearity and uniformity correction maps to provide images of excellent uniformity throughout the diagnostic range. Therefore, extending the diagnostic range to 511 keV required the extension of these linearity and uniformity correction maps into the high-energy range. The solution to this problem is manufacturer dependent and can be accomplished simply by using medium-energy maps, generating new high-energy maps or using a combination of the two (e.g., medium-energy linearity maps and high-energy uniformity maps).

Radiation leakage through the detector housing is of concern at 511 keV (tenth value layer = 13.5 mm of lead versus 0.9 mm at 140 keV), and manufacturers are now fabricating systems with shielding designed for high-energy

imaging. Evaluation of the adequacy of this shielding is a requirement in acceptance testing of new systems.

Before the need to detect 511-keV photons arose, scintillation cameras typically used 3/8 in. (9.5 mm) thick NaI(Tl) crystals because of their excellent intrinsic spatial resolution at low energies (<200 keV). However, although crystals of this thickness have a photopeak efficiency of 84% at 140 keV, the photopeak efficiency at 511 keV is only approximately 13% (*14*). Because of the need for increased efficiencies at 511 keV, manufacturers have increased the crystal sizes to 1/2 (12.7 mm), 5/8 (15.9 mm) and 3/4 in. (19.1 mm). Table 1 shows the photopeak efficiencies of different crystal thicknesses for radionuclides commonly used in nuclear medicine. The efficiency problem is much more dramatic for coincidence imaging than single-photon imaging, because both photons from an annihilation event must be detected simultaneously. Thus, the probability of detection of a coincidence event (efficiency) is the product of the two probabilities of detection (efficiencies) in the two detectors. For 3/8-in. crystals, the coincidence efficiency is 13% × 13% = 1.69%; and for 5/8-in. crystals, the coincidence efficiency is 21% × 21% = 4.41%. This is an increase by a factor of 2.6, whereas the single-detector efficiency increases only by a factor of 1.6.

If high-energy imaging were the only goal, then a thicker crystal would be the obvious choice. However, because the goal is to develop systems that can image routine low-energy single photons as well as high-energy annihilation photons, it is a potential problem that increasing the crystal thickness typically results in degraded intrinsic spatial resolution at lower energies. Recent data indicate that these degradations are not clinically significant. Table 2 shows intrinsic spatial resolutions at low energies for one commercial system (VariCam; Elscint Ltd., Haifa, Israel) using 3/8- and 5/8-in. thick crystals. When a low-energy, high-resolution collimator is used with these crystals, the measured system spatial resolution at 10 cm in air differs by only 0.2 mm for the two crystals at each of the energies. Unless the camera is very close to the imaged object, it is the collimator rather than the crystal that establishes the resolution limit.

The most significant development in scintillation camera technology that makes it possible to perform coincidence imaging is the implementation of high-counting-rate capabilities. Scintillation cameras must be able to handle extremely high single counting rates to be able to detect clinically acceptable coincidence counting rates. Much of this improvement is due to the fact that absorption of 511-keV photons results in the production of very large signals. For example, the light produced in the crystal from the total absorption of a 511-keV photon is almost four times as intense as that resulting from the total absorption of a 140-keV photon. This makes it possible to implement techniques for measuring the start of the electrical pulses that result from crystal interactions and clipping them before all of the light has been collected from each interaction. This results in the shortening of signals to a duration of approximately 200 ns instead of signals of approximately 1 μs that have been commonly used with routine single-photon emitters. This process significantly reduces the dead time introduced by each scintillation at the expense of some loss in energy resolution. Variations of this technique have been used previously by manufacturers to implement high-counting-rate modes for single-photon counting. In addition, at least one manufacturer (ADAC Laboratories, Milpitas, CA) has introduced a concept from the NaI(Tl) PET scanner that limits the number of photomultipliers used to process each event. This allows the measurement of a photon absorbed in one region of the camera to be relatively unaffected by photons absorbed in other regions of the camera. Such innovations are not typically necessary for the lower counting rates usually encountered in most gamma camera imaging situations.

The final modification required for coincidence imaging is the addition of coincidence circuitry between the two detector heads using a timing window of approximately 15 ns. This permits identification of events in which both detectors record interactions simultaneously (within 7.5 ns of each other).

PHYSICS OF DUAL-HEAD CAMERA COINCIDENCE IMAGING

Coincidence imaging using a dual-head scintillation camera is accomplished as shown in Figure 1A. The two detectors are positioned 180° from each other and rotate in unison around the region being imaged, as in routine SPECT. Conventional multihole collimators are not used, so

TABLE 1
Photopeak Detection Efficiency Versus NaI(Tl) Crystal Thickness for Radionuclides Commonly Used in Nuclear Medicine

Crystal thickness (in.)	^{201}Tl 70 keV (%)	^{99m}Tc 140 keV (%)	^{111}In 172 keV (%)	^{111}In 247 keV (%)	^{67}Ga 93 keV (%)	^{67}Ga 184 keV (%)	^{67}Ga 300 keV (%)	^{131}I 364 keV (%)	^{18}F 511 keV (%)
0.375	100	84	75	45	100	68	33	24	13
0.500	100	91	84	55	100	78	41	31	17
0.625	100	95	90	64	100	85	48	36	21
0.750	100	98	92	67	100	90	54	42	24

Adapted from (*15*).

TABLE 2
Intrinsic Spatial Resolutions (Full Width at Half Maximum of Line Spread Functions) with NaI(Tl) Crystals for Low-Energy, Single-Photon Emitters

Radionuclide	Energy (keV)	Resolution for 0.375-in. crystal (mm)	Resolution for 0.625-in. crystal (mm)
^{201}Tl	70	4.8	5.6
^{99m}Tc	140	3.8	4.3
^{18}F	511	3.1	3.3

that photons may interact with the detectors at any angle of incidence. When a positron emission occurs, the resulting annihilation radiation (two 511-keV photons) departs the site production at 180° from each other. If one of the two photons is recorded in one of the detectors, the coincidence timing window (typically 15 ns) between the two detectors is opened, and if a photon is detected in the other detector during this time interval, a coincidence event is recorded. Capturing the coordinates of the two photon interactions in the two detectors results in the determination of the annihilation process that produced the two photons and, therefore, the positron decay process occurred somewhere along a straight line defined by the two detection locations. Thus, a single coincidence event consists of the position of the detectors in their rotational orbit (to establish a reference coordinate system), the coordinates of the interaction of each photon in each detector and the pulse-height analyzer window in which each event was detected.

Ideally, the only events recorded should result from the simultaneous detection of two photons from a single annihilation process. These are termed true coincidences (Fig. 1B). However, because of the geometry of the imaging process, many of the annihilation photons do not reach the detector (Fig. 1C). This geometrical factor, as well as normal photon scatter and attenuation and the low detection efficiency of these detectors, results in many photons being detected by one detector for which corresponding photons are not detected by the opposite detector. At least 100 or more of these singles events reach each detector for each valid coincidence event. This is why cameras with high-counting-rate capabilities are required to be able to measure coincidence events with clinically acceptable sensitivity. One negative aspect of high camera rates is that as the singles rate increases, the probability increases that two photons from two separate annihilation processes will be detected by the two detectors within the coincidence timing window. This results in an invalid event with erroneous positional information, termed a random coincidence, being recorded (Fig. 1D). Thus, in the coincidence detection process, the total coincidence rate detected is the sum of both true and random coincidence events (Fig. 1E). There is no way to distinguish between true and random coincidence events. The effect of random events on image quality is to provide a background to the image that is even more broad than the background from scattered photons in coincidence or single-photon imaging. However, because random events are truly random and occur at the same rate regardless of the time difference between the two detected singles events, a separate delayed timing window can be used to measure the random coincidence rate. This value can be used to correct the random events that corrupt the in-time window.

Scatter is also of concern in coincidence imaging. If one of the two annihilation photons undergoes Compton scatter in the region being imaged but reaches the detector (Fig. 1F), the two photons will still be recorded in the coincidence timing window and an invalid coincidence event with erroneous positional information will be recorded. The performance of pulse-height analysis will eliminate the effects of large-angle scatter, but the effects of small-angle

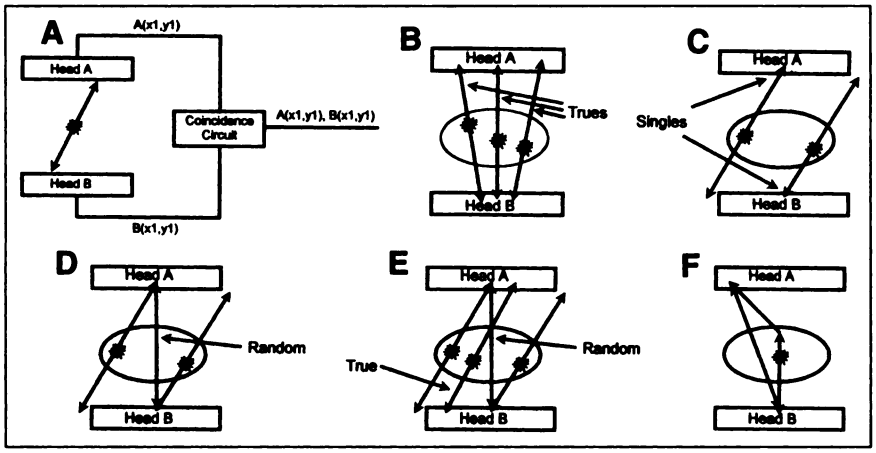

FIGURE 1. (A) Block diagram of a DHC scintillation camera system. (B) True coincidence is identified when two photons from a single annihilation process are simultaneously detected. Each detected photon is a singles event. (C) In many instances, only one photon from annihilation process is detected. (D) When two singles events from two separate annihilation processes are detected simultaneously, random coincidence is identified. (E) Total coincidence events are sum of true and random coincidences. (F) When one of two photons from a single annihilation process scatters in patient but is still detected simultaneously with unscattered photon, true coincidence with erroneous positional information is identified.

scatter will remain, as is the case with routine single-photon imaging. Unlike single-photon imaging, scattered events do not necessarily appear to come from the body.

There is also a geometrical effect that must be considered in DHC imaging with the scintillation camera. The maximum point source sensitivity is obtained when a point source is placed in the center of the field of view. As the point source is moved in any direction within the plane parallel to and equidistant from the two detectors, the point source sensitivity decreases and reaches a minimum at the edges of the plane. This decrease is caused by the reduction in solid angle from which both annihilation photons can strike the detectors and be counted. The presence of this effect requires the implementation of sensitivity profile corrections during image reconstruction to offset the reduction in sensitivity at the periphery of the field of view.

The energy spectrum from a point source of ^{18}F measured in air using a scintillation camera with a 5/8-in. (15.9 mm) thick NaI(Tl) crystal is shown in Figure 2B. The photopeak at 511 keV (energy resolution of 7.5%), the Compton edge at 350 keV and the backscatter peak at 170 keV are clearly indicated. Ideally, only photopeak events (i.e., total absorption of the 511-keV energy) occurring in the two detectors (photopeak-photopeak events) would be recorded (interaction 1 in Figure 2A) using a pulse-height analyzer window (W4) for each detector centered about the photopeak at 511 keV (Fig. 2B). However, because of the low photopeak detection efficiencies of the NaI(Tl) crystals currently available (Table 1), it is desirable to seek other methods to increase efficiency. This can be accomplished by including Compton interactions in the crystal that only result in partial absorption of the annihilation photons, as shown in Figure 2A. This is acceptable because the origin of the annihilation event and hence the location of the positron emission is determined by interactions in each of the two detectors; thus, a coincidence event may be recorded by measuring a photopeak interaction in one detector and a Compton interaction in the other detector (Fig. 2). These Compton interactions can be recorded with one or more pulse-height analyzer windows (W1–W3) covering the range from 100 to 350 keV (Fig. 2B). Some manufacturers use a single window to include the total energy range, whereas others use a single window to include only part of the range (e.g., 200–350 keV) or provide multiple windows for added versatility in pulse-height analysis. Additional sensitivity can be obtained by including coincidence events, resulting from partial absorption of both annihilation photons (interaction 3 in Fig. 2A). However, some of the events measured in the lower window(s) are photons that lost energy through scattering in the body. The inherent inclusion of these events means that lower contrast is an inevitable by-product of including photopeak-Compton and Compton-Compton events. Table 3 shows the relative increases in sensitivity that result by including these additional events when imaging a cylinder 22 cm in diameter × 20 cm long containing a uniform distribution of ^{18}F-fluorodeoxyglucose (FDG).

DATA ACQUISITION AND IMAGE RECONSTRUCTION

Data acquisition is accomplished in coincidence imaging with dual-head scintillation cameras in modes that are similar to SPECT acquisitions. The two detectors rotate around the region of interest either in continuous motion or using the step-and-shoot mode. Cameras with slip-ring technology use multiple rotations (e.g., 3 min per rotation), whereas cameras without this technology perform a single slow rotation. Total acquisition times of 20–30 min are typical in most clinical applications.

The simplest way to produce images from coincidence data is to use single-slice rebinning (SSRB) (*16*). In this method, two-dimensional projection sets like those produced in SPECT acquisitions are created from the coincidence events. Because coincidence events may deviate substantially from the transaxial plane, it is a somewhat crude approximation. Nevertheless, it allows images to be reconstructed using the same filtered backprojection software as exists on the systems for SPECT image reconstruction. Two basic improvements have been made over the

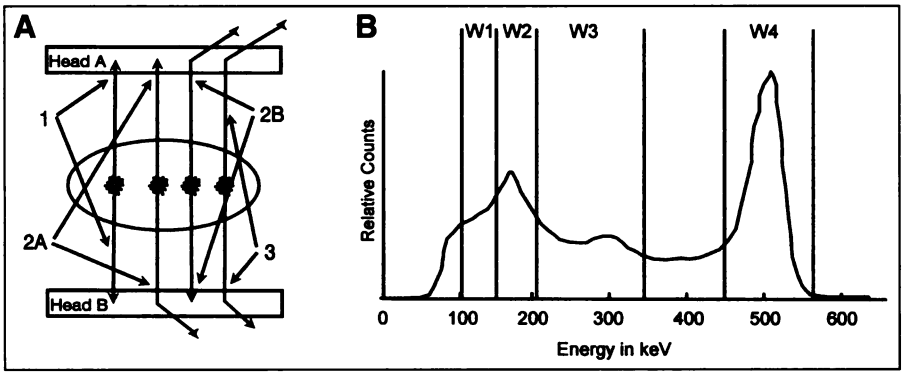

FIGURE 2. (A) Coincidence events may be defined by (interaction 1) total absorption of both annihilation photons (photopeak-photopeak), (interactions 2A and B) total absorption of one photon and partial absorption of other photon (photopeak-Compton, Compton-photopeak) and (interaction 3) partial absorption of both photons (Compton-Compton). (B) Total absorption events are detected using window (W4) positioned symmetrically around photopeak at 511 keV, and partial absorption events are detected using one or more windows (W1–W3) positioned over all or part of Compton scatter distribution in crystal (100–350 keV).

TABLE 3
Intrinsic Spatial Resolutions (Full Width at Half Maximum of Line Spread Functions) and Relative Sensitivities in Coincidence Mode with FDG

Crystal interactions included	Spatial resolution (mm)	Relative sensitivity
Photopeak-photopeak	4.5	1
Photopeak-photopeak plus photopeak-Compton	5.0	3
Photopeak-photopeak plus photopeak-Compton plus Compton-Compton	5.2	4

Measured with 22-cm diameter (times) 20-cm long uniform phantom with 0.625-in. thick NaI(Tl) crystals.

SSRB approach. One is to acknowledge the three-dimensional nature of the data, as is done with three-dimensional PET. Several image reconstruction algorithms have been developed for this purpose, resulting in improved image quality, but computer speed requirements and processing times are greater than with two-dimensional reconstruction. The other approach is to use iterative reconstruction algorithms, such as maximum likelihood-expectation (EM) and ordered subsets-EM, which have yielded improved image quality compared with backprojection. The two (three-dimensional and iterative) can be combined in one algorithm.

Because of the extremely high counting rates from singles events inherent in coincidence imaging, some manufacturers have used graded absorbers (Fig. 3A). These are thin sheets of materials of decreasing atomic number (lead > tin > copper) that absorb low-energy photons resulting from multiple scatter in the region of interest (and also characteristic x-rays produced in the absorbers (*15,17*). To further reduce the singles counting rate, various combinations of parallel lead slits (septa) have been used to limit the counting rate from annihilation events occurring outside the primary field of view (Fig. 3B). The use of these slits permits the definition of slices of activity in the region of interest from which coincidence events may be detected at any angle within the slice (Figs. 3C and 3D). The exact geometry of these slits is manufacturer dependent. They may be either fixed in place or translated in the axial direction during image acquisition to eliminate "dead" zones in acquired image data. Some septal penetration occurs, but this effect is minimized by limiting the incident angle of photons in the axial direction. The application of slit collimators is comparable with that used in two-dimensional PET in which acquisition is limited to a single plane (or adjacent planes) of detectors, and two-dimensional reconstruction algorithms are therefore more appropriate. Although DHC imaging with slit collimators is often referred to (here and elsewhere) as "two-dimensional," it should be noted that some of the acquired events deviate substantially from the transaxial plane, although much less so than is the case without such collimators.

Because coincidence imaging with dual-head scintillation cameras is performed without conventional collimators, spatial resolution is limited only by the intrinsic resolution of the camera heads. A variable that affects the spatial resolution is the angle at which a photon enters the crystal (acceptance angle), an effect that is exacerbated by increasing crystal thicknesses. This effect is due to the fact that the photon may undergo an interaction at any point along its path length through the crystal. When the incident angle is 0° (i.e., perpendicular to the crystal), there is no uncertainty in measuring the point at which the photon enters the crystal and the spatial resolution of coincidence imaging will approach the intrinsic resolution of the detector. However,

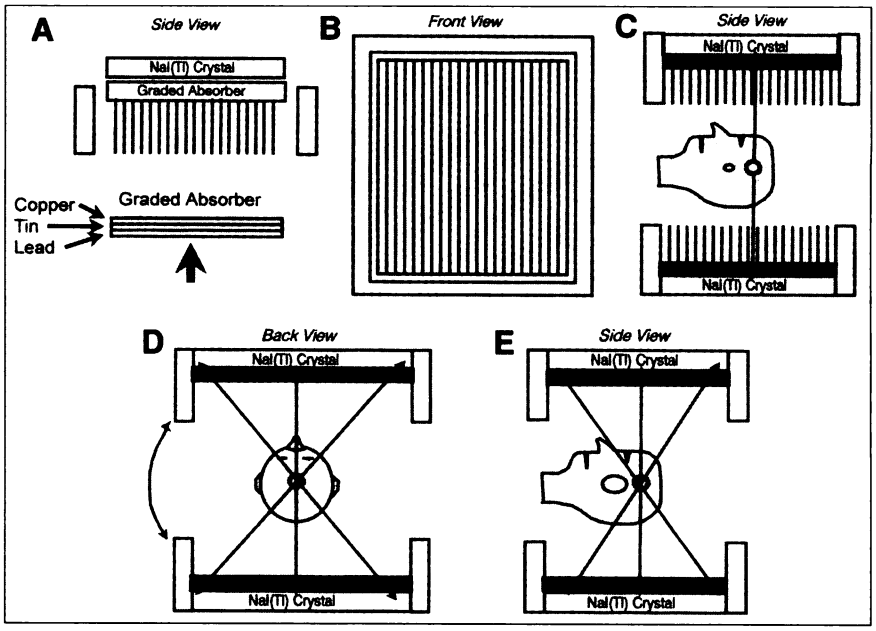

FIGURE 3. (A) In DHC imaging, graded absorbers may be used to preferentially absorb low-energy photons before they reach crystal to reduce single counting rate. (B) In two-dimensional coincidence imaging, parallel lead slits (septa) are used to define transaxial imaging slices. These slits limit acceptance of annihilation photons in axial direction to small angles (C), while permitting acceptance of photons from any angle in transaxial direction (D). In three-dimensional coincidence imaging, parallel lead slits (septa) (A) are removed so that annihilation photons may be accepted at any angle in both transaxial (D) and axial (E) directions.

for angles >0°, there is an uncertainty in locating the entry point, resulting in a degradation in spatial resolution that increases with increasing angle. This may result in a degradation in spatial resolution by as much as 40% at the maximum incident angle resulting from annihilation photons originating at the center of the field of view. On the other hand, in coincidence imaging, it is desirable to accept all incident photon angles to maximize sensitivity; thus, current systems typically ignore the slight degradations in spatial resolution and use all available acceptance angles. Typical values of spatial resolution are listed in Table 3 for a dual-head camera operating in two-dimensional coincidence mode (VariCam). The degradation in spatial resolution resulting from the inclusion of partial-absorption Compton events in the NaI(Tl) crystals is also given in Table 3. These values are comparable with those obtained with state-of-the-art dedicated PET scanners.

System sensitivity measurements for PET scanners are performed using a National Electrical Manufacturers Association (NEMA) protocol (*17,18*) that involves the measurement of coincidence events from a 20-cm diameter cylindrical phantom containing a known quantity of radioactivity and filling the entire axial field of view. However, these measurements are made under ideal conditions in which dead-time losses and random coincidence rates cannot exceed 2%; therefore, they are of limited value when evaluating the sensitivity of dual-head scintillation camera systems, which typically operate at significantly higher dead-time losses and relatively higher random coincidence rates. Of more value are counting-rate curves such as the ones shown in Figure 4. These curves were obtained by scanning a 22-cm diameter × 20-cm long cylindrical phantom with known concentrations of FDG and measuring the coincidence counting rate as a function of concentration. The random coincidence rate was also measured using a delayed timing window as described earlier, and this permits the calculation of the true coincidence counting rate. It should be noted that these curves are plotted with relative counts only on the y-axis, because the actual values are determined by the types of crystal interactions (e.g., total absorption, partial absorption) accepted in the coincidence event determinations and the counting-rate capabilities of the particular scintillation camera used to obtain the measurements. Maximum total coincidence rates in the two-dimensional mode (with slit collimators) are near 7000 coincidences/s with current systems, and rates of 3500 coincidences/s are typical for events determined by photopeak-photopeak and photopeak-Compton interactions. The true coincidence rate in this example peaks at a phantom concentration of approximately 0.35 μCi/mL and then decreases with increasing concentration. This is due to the fact that, at this phantom concentration, each detector is actually processing several hundred thousand singles events per second. As the singles rate increases, the probability of random coincidences increases and single losses (and coincidence losses) increase due to dead-time effects. Singles event losses due to dead time typically exceed 25% at the peak of the curve. Optimum image contrast (and therefore lesion detectability) of images obtained with a dual-head camera in coincidence mode typically occurs in the approximately linear portion (upslope) of the counting rate curve and may begin to degrade as the peak is approached. To illustrate this point, three images (Figs. 5A–C) of a hot sphere phantom with sphere-to-background activity ratios of 5:1 and radioactivity concentrations at different points on the upslope of the sensitivity curve are shown. There is some loss in contrast (and detectability) with the highest concentration as a result of increased random coincidences and pulse pileup effects as the optimum functional limit of the camera is approached. In clinical applications, patient doses of 148–222 MBq (4–6 mCi) FDG are considered optimum for two-dimensional coincidence imaging with this scintillation camera.

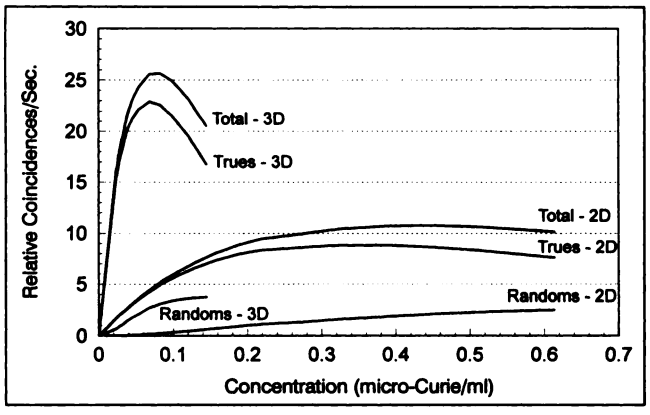

FIGURE 4. Counting-rate curves for dual-head scintillation camera operating in coincidence mode plotting relative coincidences per second (actual values depend on camera manufacturer and types of crystal absorption events used to define coincidences) versus phantom concentration for total, true and random events in two-dimensional (with slits) and three-dimensional mode for cylindrical phantom 22 cm in diameter × 20 cm long containing a uniform distribution of FDG.

Additional sensitivity can be obtained by removing the septa and increasing the acceptance angle in the axial direction to the full field of view (Fig. 3E). This mode permits the acceptance of coincidence events from any angle; thus, a true three-dimensional acquisition is accomplished. As seen in Figure 4, this results in a three-dimensional count-rate curve that rises very rapidly and peaks much earlier than the curve obtained in the two-dimensional mode. Total coincidence counting rates up to 14,000 events/s can be recorded with some systems using photopeak-photopeak and photopeak-Compton events for determining coincidence events. The use of three-dimensional acquisition reduces the maximum activity that can be within the field of view (and therefore reduces the total activity that can be in the patient at the time of imaging). Typically 74–111 MBq (2–3 mCi) FDG are used in clinical applications with camera systems operating in the three-dimensional mode. The two-dimensional approach has the

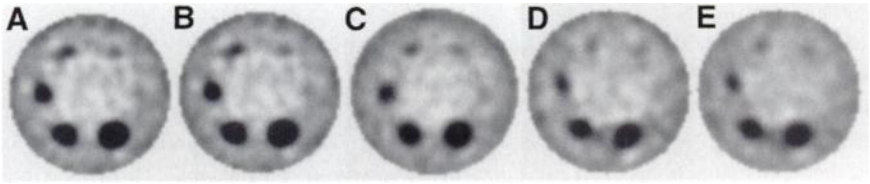

FIGURE 5. Images of hot sphere phantom in uniform background. Spheres range in diameter from 1.3 to 3.8 cm, and concentration of activity in spheres is five times that of background. Three images were obtained in 30 min in the two-dimensional mode with background concentrations of 0.077 μCi/mL (0.00285 MBq/mL) (A), 0.139 μCi/mL (0.00514 MBq/mL) (B) and 0.187 μCi/mL (0.00692 MBq/mL) (C). Two images were obtained in 30 min in three-dimensional mode with background concentrations of 0.019 μCi/mL (0.000703 MBq/mL) (D) and 0.028 μCi/mL (0.00104 MBq/mL) (E). SSRB into 90 planar projections (180°) with filtered backprojection was used to reconstruct all images.

advantage of reducing the contribution from activity outside of the field of view. The slit collimators also inhibit the detection of scattered events (scatter fraction of 14% using photopeak-photopeak events only and 29% when photopeak-Compton events are included) (Lewellen TK, personal communication) and reduced singles rate (and therefore reduced random contribution) at the expense of reduced sensitivity. The three-dimensional approach has the advantage of increased sensitivity (up to a factor of four over that of two-dimensional imaging) at the expense of increased scatter contribution (scatter fraction of 26% using photopeak-photopeak events only and 45% when photopeak-Compton events are included [Lewellen TK, personal communication]) and increased singles rate (and therefore increased random contribution). As with two-dimensional imaging, the image quality begins to degrade in three-dimensional imaging at some point near the peak of the three-dimensional counting rate curve. Figures 5D and 5E, generated using the same SSRB process described earlier for two-dimensional imaging, show some reduction in image quality compared with the images acquired in the two-dimensional mode (Figs. 5A–C), because this reconstruction process does not model three-dimensional data well. Image quality can be improved by using more complicated three-dimensional reconstruction algorithms and by applying iterative reconstruction algorithms. Even with all of these improvements, current two-dimensional PET systems still have sensitivities of 5–6 times that of DHC camera systems (*19*), a significant factor when imaging capabilities of the two techniques are compared. At least as important as sensitivity are the maximum useable coincidence counting rates, which are in the 5 kcps range for current DHC systems (without loss of image quality) and well above 100 kcps for dedicated PET systems.

ATTENUATION CORRECTION

Experience with dedicated PET scanners has shown the distortions and degradation in image quality that are inherent when the effects of attenuation are ignored (*20,21*). The effects of attenuation are much more significant in coincidence imaging than in SPECT imaging of single-photon emitters. This is due to the fact that both annihilation photons that result from a single positron-electron annihilation process must pass through the region under study without interaction for an event to be documented. The probability of this occurrence is much less than that for a single photon emitted from the same location to escape the region without interaction, even considering the lower attenuation coefficient of 511-keV photons. Reconstruction artifacts resulting from attenuation effects in coincidence imaging include regional nonuniformities, distortions of intense objects and edge effects. Thus, attenuation-correction capability is standard in dedicated PET systems, and this technology is now being applied to camera coincidence systems. The usual clinical practice in the brain is to use a calculated attenuation. This correction requires the identification of the outer contour of the head and, assuming uniform attenuation within this boundary, calculates correction factors to apply to the raw emission data. However, in the thorax, such an assumption of uniform attenuation is inappropriate, primarily because of the lungs. For the body, then, it is typical to measure the attenuation-correction factors with a transmission scan using radioactive sources. In current dedicated PET systems, this is generally accomplished using ^{68}Ge (a positron emitter) sources that rotate around the body while the scanner acquires coincidence events. In DHC camera systems, single-photon imaging techniques are more practical because of photon-detection efficiency issues. In addition, the preferred source, ^{137}Cs, emits 662-keV photons that are resolved above the 511-keV photopeak, thereby allowing transmission scanning after injection of the radiotracer (Fig. 6). Designs being implemented involve the use of point sources in fanbeam geometries, either translating across the camera or multiple sources in fixed positions on the cameras (*22–24*). With appropriate processing, the transmission data from such a system can be used to correct the emission data for attenuation effects. This results in improved image quality because of the removal of geometric distortions and nonuniform attenuation effects. This is especially true in the thorax where nonuniform attenuation effects are severe because of low-density lung tissue.

Typical artifacts are artificially bright lungs, bright body contour and dark mediastinum. A dense mass is seen in the left lung. Figure 6B is the attenuation-corrected emission image. The lung intensity is less than the surrounding tissue,

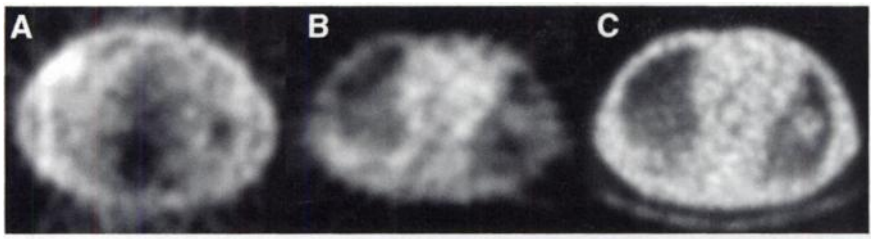

FIGURE 6. Single transaxial slice through chest of 55-y-old man injected with FDG. (A) Image was reconstructed without attenuation correction. Image (B) was reconstructed using attenuation map (C) obtained with ^{137}Cs transmission source.

as it should be, and the soft tissue regions show appropriately uniform uptake. Of particular interest is that the dense object in the left lung shows more FDG uptake than the lung tissue, which is the opposite of the uncorrected image (Fig. 6A). Moderate FDG uptake in this mass was confirmed by a dedicated PET scan of this patient.

CLINICAL APPLICATIONS

Because of the proven capabilities of dedicated PET systems in identifying and staging malignant lesions and evaluating their response to therapy, the clinical application of the greatest interest using dual-head scintillation camera coincidence imaging is in oncology. An example of the image quality currently obtainable with camera-based systems is shown in Figure 7. A 66-y-old man with a history of resected colon carcinoma and a positive CT scan of the liver was imaged with a dedicated PET scanner and a DHC camera system using two-dimensional acquisition with coincidence events determined by both photopeak-photopeak and photopeak-Compton events. The DHC images shown in Figure 7 without attenuation correction were obtained at 2.5 h postinjection of 370 MBq (10 mCi) FDG (144 MBq [3.9 mCi] at time of imaging) and demonstrated a solitary hypermetabolic liver metastasis with diagnostic image quality comparable with that of the dedicated PET system. Several investigators have reported their experience comparing lesion detection capabilities of camera systems with those of dedicated PET systems (*24–28*). A summary of experiences from one laboratory (*25,26,28*) is shown in Table 4 and is consistent with the experiences reported by other investigators. In this study, camera coincidence imaging detected 78% of all lesions detected by a dedicated PET scanner. However, when lesions were grouped according to size, camera coincidence imaging detected 68% of lesions <1.5 cm in diameter and 90% of lesions >1.5 cm. Of particular difficulty is the detection of small lesions in the abdomen, both in and outside of the liver. This is because even though camera coincidence systems have the spatial resolution of PET, they do not have the sensitivity of dedicated PET systems, and therefore, small lesions are more often lost in the noise. Thus, in the absence of a dedicated PET system, it may be appropriate to use current DHC cameras in some oncological applications as long as the limitations of these systems are clearly understood. Attenuation correction may improve detection of some lesions.

The imaging capabilities of DHC camera systems in brain imaging are demonstrated in Figure 8. A 36-y-old woman with a history of refractory seizures was studied at 51 min postinjection of 370 MBq (10 mCi) FDG with a DHC camera system using two-dimensional acquisition, with coincidence events determined by both photopeak-photopeak and photopeak-Compton events. The images shown in Figure 8 without attenuation correction demonstrate decreased uptake in the right temporal lobe consistent with interictal seizure focus in that region. Clinical information obtained with the DHC camera system was comparable with that obtained with a dedicated PET scanner, although the image quality was not as good because of the decreased sensitivity of the camera system.

In cardiac imaging, the sensitivity of DHC camera imaging is sufficient to obtain images of diagnostic quality, but attenuation correction is a necessity. Figure 9 shows selected vertical long-axis views of a patient imaged with routine collimated SPECT using a high-energy collimator (Figs. 9A and B) and with coincidence detection (Fig. 9C). These images were obtained simultaneously using a dual-

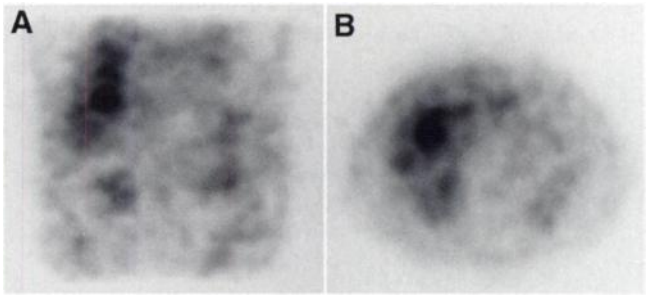

FIGURE 7. Selected coronal (A) and transverse (B) views (FDG) of 66-y-old man with metastatic lesion in liver from colon carcinoma. Images were acquired in 30 min in two-dimensional mode with dual-head scintillation camera operating in coincidence mode.

TABLE 4
Percentage of Lesions Detected by Dedicated PET System that Were also Identified by Dual-Head Scintillation Camera Coincidence Imaging

Lesion location	Lesion <1.5 cm (%)	Lesion >1.5 cm (%)	All lesion sizes (%)
Thorax	78	100	83
Liver	43	100	67
Extrahepatic abdominal	0	78	78
All locations	68	90	78

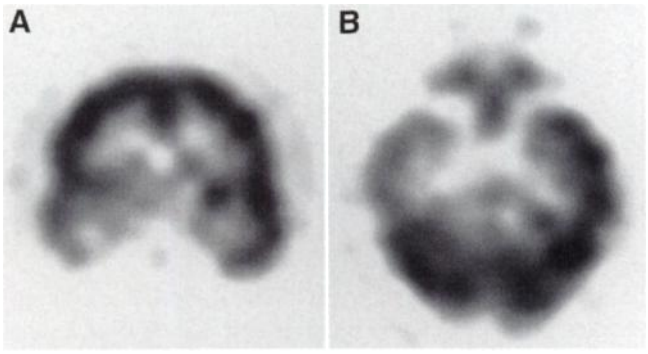

FIGURE 8. Selected coronal (A) and transverse (B) views (FDG) of the brain of 36-y-old woman with right temporal lobe epilepsy. Images were acquired in 30 min in two-dimensional mode with dual-head scintillation camera operating in coincidence mode.

isotope, single-acquisition (DISA) SPECT protocol (*11,12*). Comparing the image of the FDG distribution (Fig. 9C) with the SPECT image (Fig. 9B), it is apparent that the decreased metabolism is actually caused by attenuation effects and not disease. Thus, as discussed earlier, attenuation effects are much more severe in coincidence imaging than in the imaging of single photons. Therefore, attenuation correction must be performed in cardiac imaging using DHC camera systems. It should also be noted that Figures 9A and B are of excellent diagnostic quality, although the spatial resolution of the DHC technique is clearly superior. Because of the ability of the DISA SPECT protocol to simultaneously evaluate perfusion and metabolism, this technique is currently preferred to DHC imaging of the myocardium.

ITERATIVE RECONSTRUCTION TECHNIQUES

The most commonly used technique for image reconstruction in SPECT is filtered backprojection, and therefore, it was logical to initially make use of this technique in the reconstruction of image data from DHC camera systems. However, this technique amplifies statistical noise that adversely affects image quality. Shepp and Vardi (*29*) introduced an iterative reconstruction technique in 1982 based on the theory of EM, which has a proven theoretical convergence to an estimate of the actual image distribution that has a maximum likelihood of having projections most similar to the acquired projections. The use of these algorithms was time consuming, with several iterations required to reach a solution, and extensive computer power was required. Since that time, much effort has been expended in improving and testing algorithms based on this concept. Significant improvements in speed, signal-to-noise and reconstruction accuracy have resulted from these efforts, and variations of this concept are now being used in iterative reconstruction algorithms for data from DHC camera systems. Because the data acquired from these systems are truly three-dimensional in nature, it is possible to couple a three-dimensional image reconstruction algorithm with these iterative techniques that optimize spatial resolution while reducing the effects of statistical noise. An approach like this can be implemented with attenuation and sensitivity profile corrections built into the algorithm and performed during the image reconstruction process, resulting in images that are more accurate in their representation of the distribution under study.

FUTURE IMPROVEMENTS

As discussed earlier, the primary limitations of DHC imaging with the scintillation camera are sensitivity and the related coincidence counting-rate limits. Several techniques for increasing sensitivity are being evaluated. One obvious improvement is to increase crystal thickness; however, this solution will result in degraded spatial resolution in the collimated imaging of low-energy single-photon emitters. An alternative is to alter the makeup of the detectors. Currently, combinations of detectors materials such as lutetium orthosilicate (LSO) and yttrium orthosilicate (YSO) are being developed that significantly improve decay times (40 and 70 ns, respectively) compared with conventional NaI(Tl) (230 ns) (*22*). When sandwiched in layers, these two materials can be used together in a multipurpose detector system for both low-energy (YSO) and high-energy (LSO) imaging with improved efficiency. If many small detectors are used instead of single large-area detectors, as with current scintillation cameras, significant gains in counting-rate capability can be obtained by parallel signal detection and processing. Solid-state detectors using materials such as cadmium-zinc-telluride (CdZnTe) are currently under development (*30*), which also have the potential for improved sensitivity and high-counting-rate capability.

Another obvious improvement in sensitivity would be to

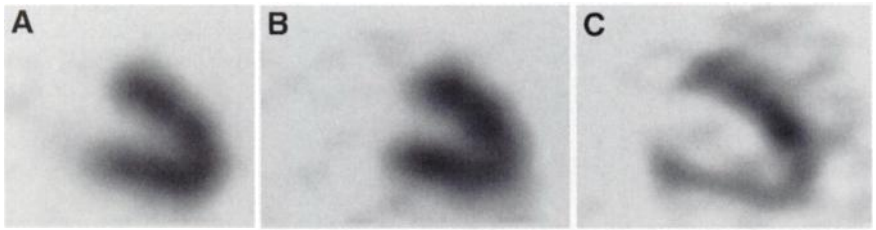

FIGURE 9. Selected vertical long-axis views of heart of 56-y-old man with normal perfusion (^{99m}Tc-sestamibi) (A) and normal metabolism (FDG) (B) imaged with SPECT camera equipped with high-energy collimator and using DISA protocol. (C) Image of FDG distribution obtained before administration of ^{99m}Tc-sestamibi with dual-head scintillation camera operating in coincidence mode without attenuation demonstrates apparent decrease in metabolism in inferior wall.

add a second set of detectors, which would also significantly increase cost. One manufacturer (Picker International, Cleveland, OH) currently uses three detectors, pairing them electronically for coincidence imaging. This possibility of further increasing the number of detectors and/or changing database materials (as well as transmission scanning requirements for attenuation correction) raises the question of whether substantial effort should be devoted to the development of a multipurpose scintillation camera system that will probably be more expensive than systems currently available or be spent on improving conventional dedicated PET systems with one of the goals to reduce the cost. The answer to this question is not obvious at present, and efforts will continue on both of these options until the limitations of each are better defined.

CONCLUSION

Most scintillation camera manufacturers are now offering multihead scintillation cameras with DHC imaging capability. The spatial resolutions of these systems rival those of dedicated PET scanners; however, DHC systems are currently limited in sensitivity and counting rates compared to PET systems. This limitation is evident in the imaging of small lesions (<1.5 cm). Continued developments will close the gap in sensitivity but will probably not overcome the sensitivity advantage of PET systems. It is only when clinical evaluations of these improved camera systems become available that the question of whether they are adequate to replace dedicated PET scanners in all clinical imaging situations will be answered.

ACKNOWLEDGMENTS

We acknowledge grant support from ELGEMS, Inc., Haifa, Israel. We thank Amy York for editorial assistance and John Bobbitt for photographic assistance. In addition, group support from the physicians and basic scientists in nuclear medicine at Vanderbilt University Medical Center and Duke University Medical Center is greatly appreciated.

REFERENCES

1. Brownell GL, Sweet WH. Localization of brain tumors with positron emitters. *Nucleonics*. 1953;11:40–45.
2. Anger HO. Scintillation camera. *Rev Sci Instr*. 1958;29:27–33.
3. Anger HO. Gamma-ray and positron scintillator camera. *Nucleonics*. 1963;21:56–59.
4. Anger HO, Rosenthal DJ. Scintillation camera and positron camera. In: *Medical Radioisotope Imaging*. Vienna, Austria: International Atomic Energy Agency, 1959:59–82.
5. Muehllehner G. Positron camera with extended counting rate capability. *J Nucl Med*. 1975;16:653–657.
6. Muehllehner G, Buchin MP, Dudek JH. Performance parameters of a positron imaging camera. *IEEE Trans Nucl Sci*. 1976;23:528–537.
7. Ter-Pogossian MM, Phelps ME, Hoffman EJ, et al. A positron-emission transaxial tomograph for nuclear imaging (PETT). *Radiology*. 1975;114:89–98.
8. Karp JS, Muehllehner G, Mankoff DA, et al. Continuous-slice PENN-PET: a positron tomograph with volume imaging capability. *J Nucl Med*. 1990;31:617–627.
9. Glass EC, Nelleman P, Hines, H, et al. Initial coincidence imaging experience with a SPECT/PET dual-head camera [abstract]. *J Nucl Med*. 1996;37:53P.
10. Miyaoka RS, Costa WLS, Lewellen TK, et al. Coincidence mode imaging using a standard dual-headed gamma camera [abstract]. *J Nucl Med*. 1996;37:223P.
11. Patton JA, Hefetz Y, Shone MD, Stoner MB, Sandler MP. Measured coincidence imaging parameters of a clinical dual-head scintillation camera [abstract]. *J Nucl Med*. 1997;38:221P.
12. Sandler MP, Videlefsky S, Delbeke D, et al. Evaluation of myocardial ischemia using a rest metabolism/stress perfusion protocol with ^{18}FDG/ ^{99m}Tc-MIBI and dual isotope simultaneous acquisition SPECT. *J Am Coll Cardiol*. 1995;26:870–878.
13. Sandler MP, Bax JJ, Patton JA, Visser FC, Martin WH, Wijns W. Fluorine-18-fluorodeoxyglucose cardiac imaging using a modified scintillation camera. *J Nucl Med*. 1998;39:2035–2043.
14. Anger HO, Davis DH. Gamma-ray detection efficiency and image resolution in sodium iodide. *Rev Sci Instr*. 1964;35:693.
15. Muehllehner G, Jaszczak RJ, Beck RN. The reduction of coincidence loss in radionuclide imaging cameras through the use of composite filters. *Phys Med Biol*. 1974;19:504–510.
16. Daube-Witherspoon ME, Muehllehner G. Treatment of axial data in three-dimensional PET. *J Nucl Med*. 1987;28:1717–1724.
17. National Electrical Manufacturers Association. *Performance Measurements of Positron Emission Tomographs*. NEMA Standards Publication NU 2–1994. Washington, DC: National Electrical Manufacturers Association, 1994:13.
18. Karp JS, Daube-Witherspoon ME, Hoffman EJ, et al. Performance standards in positron emission tomography. *J Nucl Med*. 1991;32:2342–2350.
19. Budinger TF. PET instrumentation: what are the limits? *Semin Nucl Med*. 1998;28:247–267.
20. Huang S-C, Hoffman EJ, Phelps ME, et al. Quantitation in positron emission computed tomography: 2. Effects of inaccurate attenuation correction. *J Comput Assist Tomogr*. 1979;3:804–814.
21. Zasadny KR, Kison PV, Quint LE, et al. Untreated lung cancer quantification of systematic distortion of tumor size and shape on non-attenuation-corrected 2-[fluorine-18]fluoro-2-deoxy-n-glucose PET scans. *Radiology*. 1997;201:873–876.
22. Laymon CM, Turkington TG. Attenuation effects in camera coincidence imaging. *IEEE Trans Nucl Sci*. 1998;45:3115–3121.
23. Laymon CM, Turkington TG, Gilland DR, et al. Transmission scanning on a gamma camera coincidence imaging system [abstract]. *J Nucl Med*. 1998;39:92P.
24. Coleman, RE, Laymon CE, Turkington TG. Positron imaging of pulmonary nodules: phantom study [abstract]. *J Nucl Med*. 1998;39:108P.
25. Sandler MP, Delbeke D, Patton JA, Martin WH, Vithalani R, Balan R. Comparison of FDG PET and coincidence ECT imaging using a dual-head scintillation camera in patients with suspected malignancies [abstract]. *Eur J Nucl Med*. 1997;24:860.
26. Delbeke D, Sandler MP, Al-Sugair A, et al. Comparison of dedicated and camera-based PET imaging of FDG in patients with focal pulmonary lesions [abstract]. *J Nucl Med*. 1998;39:108P.
27. Schreve P, Steveton RS, Deters E, et al. Lesion detection in oncologic diagnosis: comparison of dual-head coincidence with dedicated PET FDG imaging [abstract]. *J Nucl Med*. 1998;39:109P.
28. Delbeke D, Patton JA, Martin WH, Sandler MP. FDG PET and dual-head gamma camera positron coincidence detection imaging of suspected malignancies and brain disorders. *J Nucl Med*. 1999;40:110–117.
29. Shepp LA, Vardi Y. Maximum likelihood reconstruction for emission tomography. *IEEE Trans Med Imaging*. 1982;1:113–122.
30. Kipper M, Yeung D, Halpern S, et al. Quality of planar images using a solid-state (CdZnTe) gamma camera, compared with conventional gamma scintillation cameras [abstract]. *J Nucl Med*. 1998;39:132P.